

Geomagnetically Induced Currents, a space weather hazard. Case study - Europe under intense geomagnetic storms of the solar cycle 23

Venera Dobrica, Crisan Demetrescu, Cristiana Stefan, Razvan Greculeasa

Institute of Geodynamics, Romanian Academy,

E mail (venera@geodin.ro).

Accepted : 26 January 2016

Abstract. The interaction of the solar wind and heliospheric magnetic field with the magnetosphere and ionosphere results in variations of the geomagnetic field that induce hazardous electric currents in grounded technological systems (electric power and hydrocarbon transportation networks), the so-called geomagnetically induced currents (GICs). In order to evaluate the hazard induced on the European continent, we present a study of the surface electric field induced by 16 intense ($Dst < -150$ nT) geomagnetic storms, based on the analysis of the geomagnetic records from the European network of observatories, study that tend to solve the geophysical part of the problem. The evolution during storm development and the sources of the disturbance field are explored in case of the largest geomagnetic storm in the cycle 23 ($Dst = -422$ nT, November 20-21, 2003), and the geographical distribution of the maximum induced surface geoelectric field over Europe by the 16 storms considered in the study is presented. As source proxies, the Dst geomagnetic index, showing the disturbed field produced by the magnetospheric ring current at the geomagnetic equator, the AL geomagnetic index, showing the disturbed field produced by the ionospheric electrojet at auroral latitude, and the PC geomagnetic index, showing the disturbed field produced by the polar cap current, were examined.

© 2016 BBSCS RN SWS. All rights reserved

Keywords: intense geomagnetic storms of solar cycle 23, sources of geomagnetic variation, surface geoelectric field over Europe

Introduction

The influence of eruptive solar processes over the Earth is a subject of great importance in present times in the context generated by satellite space missions that study both the Sun and the heliosphere. The first observation of an eruptive phenomenon – a strong flare in white light – with geomagnetic consequences was that one made independently by Carrington (1859) and Hoggson (1859).

The strong variations of the magnitude and direction of the geomagnetic field during geomagnetic storms and substorms triggered by the interaction with the magnetosphere and ionosphere of coronal mass ejections (CMEs), mainly during the maximum solar activity (Hildener et al., 1976; Gopalswamy, 2004), and by the high speed streams (HSSs) in the solar wind, especially in the declining phase of the 11-year solar cycle (Gosling et al., 1971; Bame et al., 1976), induce in the Earth and in the power grid systems certain variable electric fields that produce, in turn, electric currents known as geomagnetically induced currents (GICs). This current type has been studied since the middle of the 19th century, following observations from communication cables. In the years following the catastrophic breakdown of the power network in Quebec, Canada, during the severe magnetic storm of March 13/14, 1989, a special interest has been given to induced currents both in Canada and in the northern countries (Blais and Metsa, 1994; Boteler and Pirjola, 1998; Viljanen, 1997; Pirjola and Viljanen, 1998; Beamish et al., 2002; Wei et al., 2013), as being most affected by such a phenomenon because of the proximity of the

auroral current system. On the other hand, it has been shown that the effects of induction could be significant at more southern latitudes (British Isles, South Africa) (Beamish et al., 2002; Beggan et al., 2013). Having in view the harmful potential, with great social and economic impacts, of an extreme space weather event, both at high latitudes and at low and middle latitudes, recently, many studies have focused on assessing the possible impact of GICs on the ground-based conductor networks using complex methods (Liu et al., 2014; Matandirotya et al., 2015; Torta et al., 2015; Watari et al., 2015).

The computation of GIC in a given system of conductors is done in two steps: (1) the determination of the electric field associated to geomagnetic variations, step that does not depend on the concrete technological system, and (2) the determination of GIC in the given technological system. In the present paper we concentrate on the geophysical part of evaluating this type of space weather hazard, namely on determining surface electric field, at the European scale, based on recordings from the European geomagnetic observatories network during 16 intense ($Dst < -150$ nT) geomagnetic storms. The largest geomagnetic storm of the solar cycle 23 ($Dst = -422$ nT, November 20-21, 2003) was investigated as regards the evolution of the induced electric field during the storm and the contribution of solar wind and magnetospheric ring current to the observed geomagnetic disturbances.

Data and method

The largest storm of the solar cycle 23, namely – November 20-21, 2003, Dst = -422 nT – was initiated by the interaction with the magnetosphere of an interplanetary coronal mass ejection (ICME) (November 20, 2003, 08:03 UT), observed in the interplanetary space as a result of a halo CME registered on November 18, 2003, at 10:24 UT, as seen in the LASCO (Large Angle and Spectrometric Coronagraph) instrument images from SOHO mission (Solar and Heliospheric Observatory) (Private communication, Diana Ionescu, 2015). The solar wind parameters (total heliospheric magnetic field, B, Bz component, density, velocity and dynamic pressure, N, V, and respectively Pw) recorded at the Lagrangean point L1 for the time interval November 18-23, 2003, available at <http://omniweb.gsfc.nasa.gov/>, as 1-minute data, were used in this paper to show interplanetary medium conditions.

The disturbed magnetic field observed at the surface of the Earth during magnetic storms is the sum of the effect of disturbed electric currents (Cole, 1966). The geomagnetic indices related to various magnetospheric and ionospheric currents represent good means to characterize space weather events. To explain the observed disturbances of the geomagnetic field and relation with their sources, during the analyzed geomagnetic storm,

geomagnetic indices such as the Dst geomagnetic index (<http://wdc.kugi.kyoto-u.ac.jp/>), showing the disturbed field produced by the magnetospheric ring current at the geomagnetic equator, the AL geomagnetic index (<http://omniweb.gsfc.nasa.gov/>), showing the disturbed field produced by the ionospheric electrojet at auroral latitude, and, the PC geomagnetic index (<http://omniweb.gsfc.nasa.gov/>), showing the disturbed field produced by the polar cap current, were examined.

1-minute values of the northward and eastward geomagnetic elements, recorded at up to 29 European observatories from the INTERMAGNET network (<http://www.intermagnet.net/>), listed in Table 1, during six days encompassing the 16 intense storms of the study (Table 2), were processed to get the time derivative that is driving the induced electric field.

The induced electric field is assessed according to the method of Viljanen and Pirjola (1989), shortly reviewed in the next lines.

Generally, the horizontal electric field (E_x , E_y) produced by the variable magnetic field is linked to the magnetic field (B_x , B_y) through the impedance $Z(\omega)$ of the underground subject to the plane wave that approximates the propagation of the geomagnetic disturbance.

Table 1. Geographic and geomagnetic coordinates of geomagnetic observatories

No.	Observatory (IAGA code)	Geographic coordinates		Geomagnetic coordinates	
		Latitude (°)	Longitude (°)	Latitude (°)	Longitude (°)
1	SFS	36.66	354.06	39.92	73.68
2	SPT	39.55	355.65	42.46	76.13
3	EBR	40.82	0.50	42.88	81.43
4	PAG	42.52	24.18	40.44	105.09
5	GCK	44.63	20.77	42.86	102.45
6	SUA	44.68	26.25	42.20	107.68
7	THY	46.90	17.90	45.84	100.19
8	NCK	47.63	16.71	46.68	99.68
9	HRB	47.87	18.18	46.66	101.17
10	CLF	48.02	2.27	49.65	85.37
11	FUR	48.17	11.28	48.14	96.66
12	BDV	49.08	14.01	48.55	97.65
13	DOU	50.10	4.60	51.16	88.91
14	MAB	50.30	5.68	51.17	90.06
15	HAD	51.00	355.52	53.6	80.17
16	BEL	51.83	20.80	50.06	105.18
17	VAL	51.93	349.75	55.47	74.61
18	NGK	52.07	12.68	51.66	97.63
19	WNG	53.75	9.07	53.89	94.95
20	HLP	54.60	18.82	53.06	104.59
21	ESK	55.32	356.80	57.52	83.66
22	BFE	55.63	11.67	55.25	94.81
23	BOX	58.06	38.21	53.32	123.59
24	UPS	59.90	17.35	58.35	106.16
25	LER	60.13	358.82	61.74	88.78
26	NUR	60.52	24.65	57.74	113.05
27	LYC	64.60	18.75	62.35	110.82
28	SOD	67.37	26.63	63.87	119.75
29	ABK	68.35	18.81	65.98	114.33

Table 2. The studied intense geomagnetic storms of solar cycle 23

Year	Date	Dst (nT)	Year	Date	Dst (nT)
1998	May, 4	-205	2001	Apr, 11	-271
1998	Sep, 25	-207	2001	Nov, 5	-292
1999	Oct, 21	-237	2001	Nov, 24	-221
2000	Apr, 6	-287	2003	Oct, 29	-383
2000	Jul, 15	-301	2003	Nov, 20	-422
2000	Aug, 12	-235	2004	Nov, 7	-374
2000	Sep, 17	-201	2005	May, 15	-247
2001	March, 31	-387	2005	Aug, 24	-184

$$E_x(\omega) = \frac{Z(\omega)}{\mu_0} B_y(\omega), E_y(\omega) = \frac{Z(\omega)}{\mu_0} B_x(\omega) \quad (1)$$

For an Earth viewed as a halfspace with a conductivity σ , the surface electric field is described by

$$E_y(t) = -\frac{1}{\sqrt{\pi\mu_0\sigma}} \int_{-\infty}^t \frac{g_x(u)}{\sqrt{t-u}} du \quad (2)$$

where g_x denotes the time derivative of the field B. The integral is converted to a sum that allows to calculate the 1-minute E values. A rather simple numerical code was written for getting induced electric field values. As the input parameters we used the electrical conductivity and 1-minute time derivative of the north and east components of the geomagnetic field from each observatory, during six days time interval (8640 data) that includes the geomagnetic storm. Based on eq. (2), we got as output the components of the electrical field.

Two other more sophisticated methods to estimate the geographical distribution of the induced geoelectric field in a denser network of points are presently in use (Viljanen et al., 2014; Matandirotya et al., 2015). These approaches are based on the method of spherically elementary current systems applied for a layered Earth's conductivity model, and, respectively, on the finite element method applied for realistic Earth's conductivity profiles.

Results and discussion

The interplanetary medium parameters during the time interval November 18-23, 2003, (the geomagnetic storm included) are illustrated in Fig. 1. The total heliospheric magnetic field, B, the Bz component, the density, velocity and dynamic pressure, N, V, and respectively Pw are shown. The evolution of the storm is illustrated in the same figure by means of the Dst geomagnetic index.

To get an idea on the latitudinal differences that characterize the evolution of the geomagnetic field and of its time derivative, as well as of the induced surface geoelectric field during a geomagnetic storm, we show in Fig. 2 the results obtained for a longitudinal chain of observatories. The chain of observatories is along the 105°E geomagnetic meridian. To show the

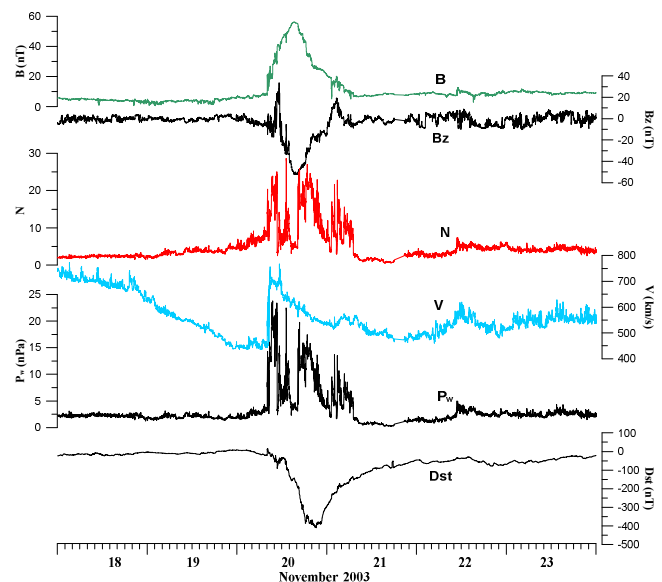


Fig. 1. Solar wind parameters and the Dst evolution for the November 2003 storm

extreme possible variations, the AL geomagnetic index, showing the disturbed field produced by the ionospheric electrojet at auroral latitude, and the Dst index, showing the disturbed field produced by the magnetospheric ring current at the geomagnetic equator, are plotted on top and, respectively, at the figure bottom.

Examining the figure several conclusions can be underlined, namely:

- the disturbance in Bx is 2-3 times larger at northern latitudes than at mid and southern latitudes;
- during the geomagnetic storm, effects of auroral electrojets superimpose at all latitudes on the disturbance created by the magnetospheric ring current;
- the amplitude of the geoelectric field produced by magnetic variations is of the order of hundredths mV/km in case of SUA (45°N), and of 1-2 mV/km in case of UPS (60°N);
- the more pronounced geoelectric component is directed East-West, as a consequence of the fact that the geomagnetic disturbance is more pronounced in the northward component of the geomagnetic field than in the eastward one.

The surface electric field at the European observatories considered in the present study was calculated for various moments of the storm development in its initial and main phases, marked in Fig. 3. In the left panel the evolution of the electric field at a mid-latitude observatory (HRB – Hurbanovo) is presented as an example, and in the right panel the Dst index was plotted. For each of the moments marked in Fig. 3 by vertical lines, maps of the surface electric field were drawn, of which we give a few examples in Fig. 4.

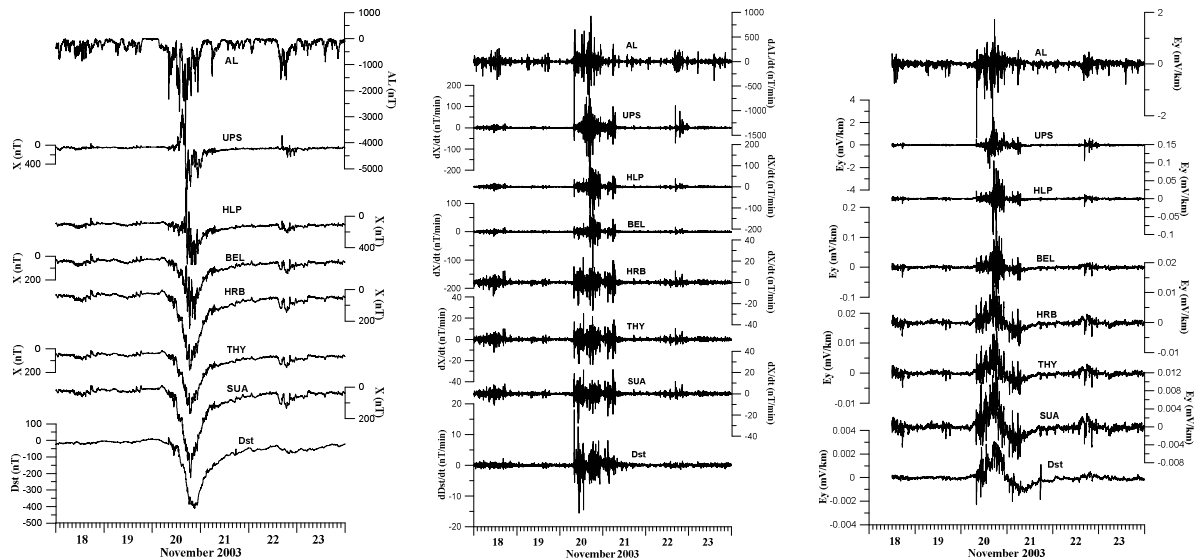


Fig. 2. The geomagnetic disturbance (Bx) (left), its time derivative (middle), and the resulting surface electric field (Ey) (right) for the November 2003 storm, at geomagnetic observatories along the 105° E geomagnetic meridian

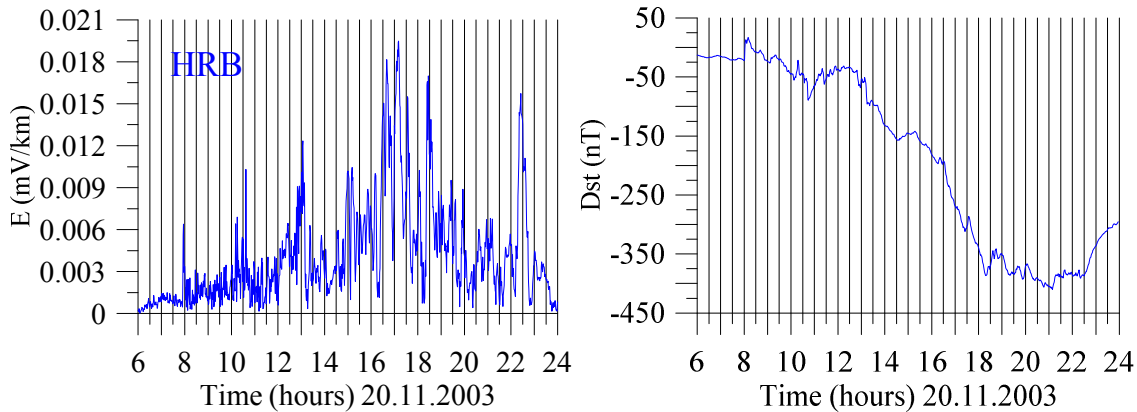


Fig. 3. The evolution of the November 2003 geomagnetic storm in its initial and main phases through the surface electric field at HRB (left plot) and Dst index (right plot). Vertical lines indicate moments for which maps of the electric field were drawn

The maps show that (1) the largest disturbances occur in Scandinavia, and to a lesser extent, in England, and (2) the direction of the electric field is highly variable during the storm and is not necessarily the same at all points at a certain moment of the storm.

As regards the sources of the variations observed, our study indicates both the magnetospheric ring current and the ionospheric auroral electrojet. Fig. 5 shows the geographical distribution of the correlation coefficient between the observed geomagnetic disturbance and the Dst index, while Fig. 6 shows that in case of northern latitude observatories the auroral electrojet and sometimes the magnetopause currents produced by solar wind pressure impulses are a good candidate.

Finally, as a next step in assessing the GIC hazard for the European territory, we calculated the maximum value of the electric field and its orientation at observatories of the network, for each storm considered in this study. Maps are presented in Fig. 7.

It is to be noted that the maximum E value is not reached at the same moment at all observatories and its orientation depends on that moment of the storm development. Estimating the actual GICs is an engineering problem and needs knowledge of the power grid.

Conclusions

The geophysical part of evaluating, at the European scale, the space weather hazard produced by geomagnetically induced currents was approached by determining the surface electric field during 16 intense ($Dst < -150$ nT) geomagnetic storms in the solar cycle 23. The study is based on recordings from the European geomagnetic observatories network. The largest geomagnetic storm of the solar cycle 23 ($Dst = -422$ nT, November 20-21, 2003) was investigated as regards the evolution of the induced electric field during the storm and the contribution of solar wind and magnetospheric ring current to the observed geomagnetic disturbances. The latitudinal

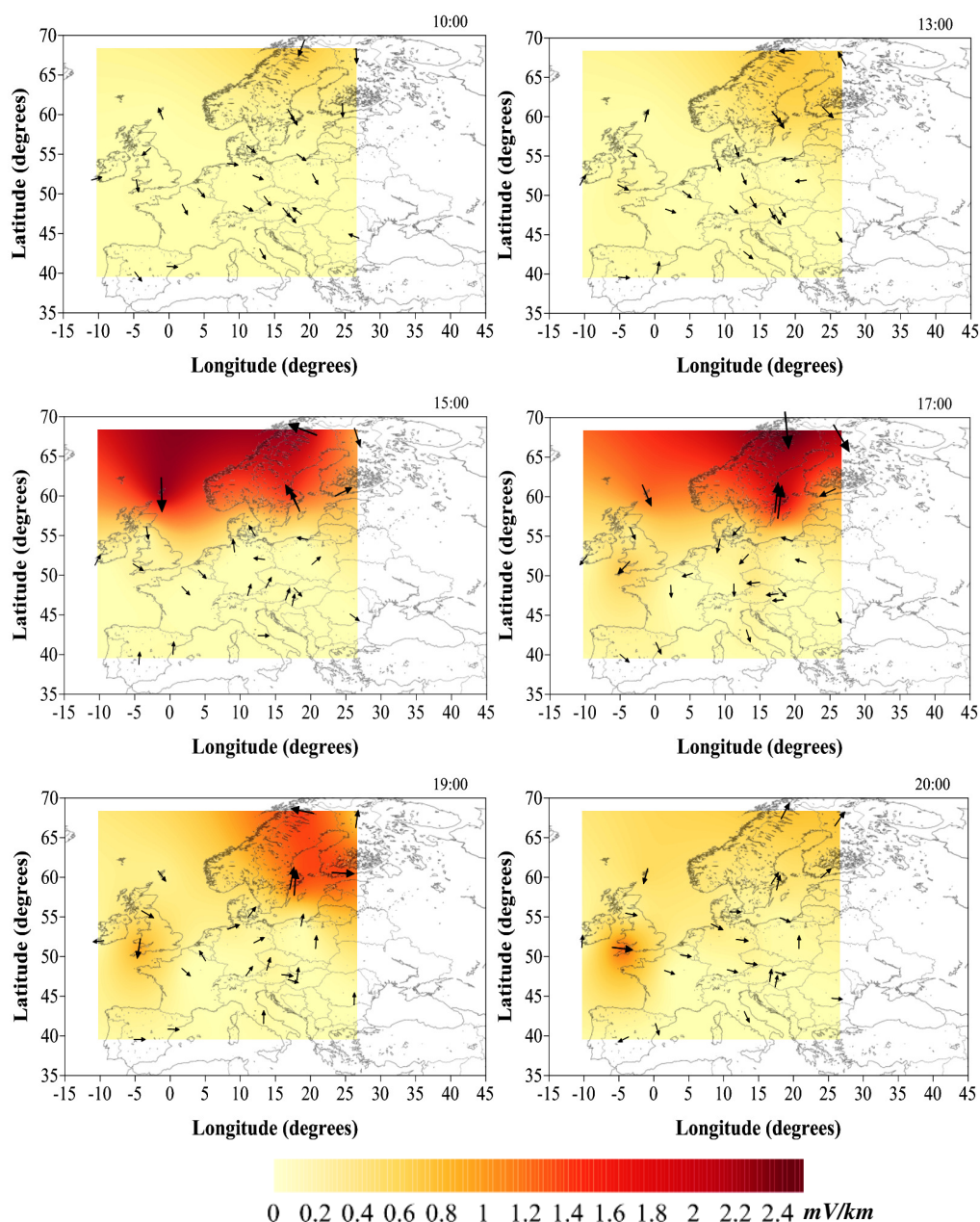


Fig. 4. Snapshots of surface electric field maps during the initial and main phases of the November 2003 storm, for moments marked on each map. The orientation of the field is given by arrows, and the magnitude by both colors and arrows length

dependence of the storm effects was investigated for the case of a longitudinal chain of observatories along the 105°E geomagnetic meridian.

Latitudinal differences in the observed effects of the November 20-21, 2003 storm refer to the magnitude of the geomagnetic disturbance and the corresponding electric field, as well as to the sources of the disturbances, as follows:

- the disturbance in B_x is 2-3 times larger at northern latitudes than at mid and southern latitudes;
- the amplitude of the geoelectric field produced by magnetic variations is of the

order of hundredths mV/km in case of SUA (45°N), and of 1-2 mV/km in case of UPS (60°N);

- during the geomagnetic storm, effects of auroral electrojets superimpose at all latitudes on the disturbance created by the magnetospheric ring current, but are more pronounced in Scandinavia and to a lesser extent in England. In Central and Southern Europe effects of the magnetospheric ring current variations dominate;
- in case of northern latitude observatories, besides the auroral electrojets, the magnetopause currents produced by solar

wind pressure impulses are sometimes a good candidate as source of variations observed.

Further work will include looking at local effects and exploring the role of magnetopause currents produced by solar wind pressure impulses as well as electrodynamical coupling between high and low latitudes. Estimating the actual GICs is an engineering problem and needs knowledge of the power grid.

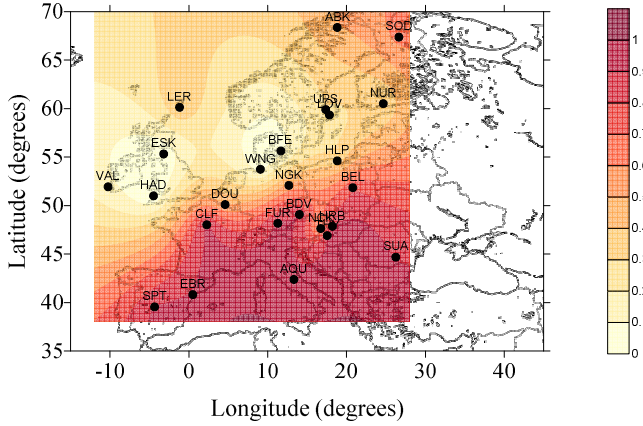


Fig. 5. Correlation coefficient between the Dst index and the horizontal component disturbance at European observatories

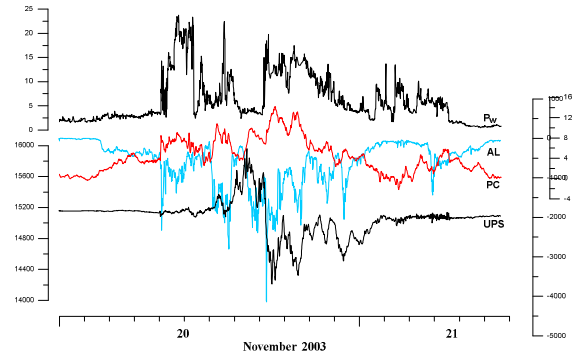


Fig. 6. Evolution of the solar wind dynamic pressure P_w , polar cap currents (PC index), auroral electrojet (AL index), and geomagnetic disturbance at a northern observatory (UPS)

Acknowledgements.

The study has been done in the frame of the project CNCSIS – UEFISCDI 93/2011.

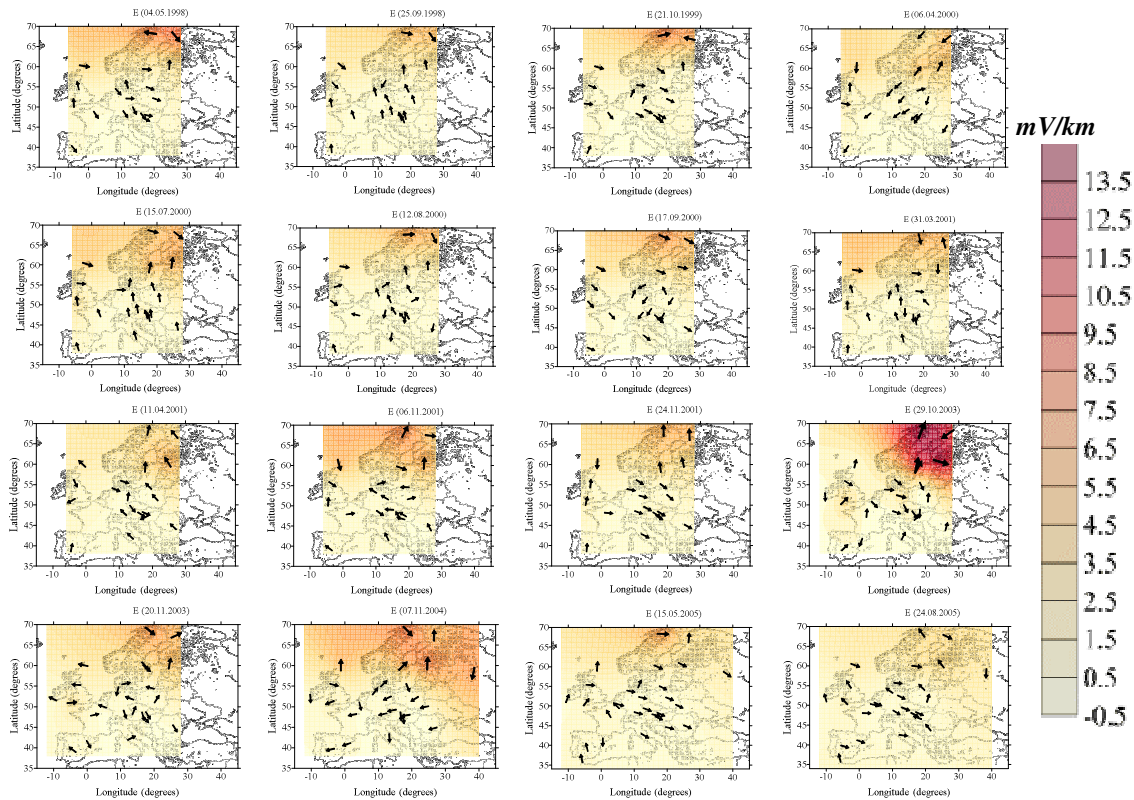


Fig. 7. Maps of the maximum geoelectric field induced at observatories of the European network, for each of the 16 geomagnetic storms of the present study

References

- Carrington, R.: 1859, *Monthly Notices of the Royal Astronomical Society* 20, 13.
- Cole, K.D.: 1966, *Space Science Reviews* 5, 699.
- Bame, S.J., Asbridge, J.R., Feldman, W. C. and Gosling, J.T.: 1976, *Astrophysical Journal* 207, 977.
- Beamish, D., Clark, T.D.G., Clarke, E. and Thomson, A.W.P.: 2002, *J. Atmos. Sol. Terr. Phys.* 64, 1779, doi:10.1016/S1364-6826(02)00127-X.
- Beggan, C.D., Beamish, D., Richards, A., Kelly, G.S. and Thomson, A.W.P.: 2013, *Space Weather* 11, 407, doi:10.1002/swe.20065.
- Blais G. and Metsa P.: 1994, *Solar-Terrestrial Predictions IV*, 108.
- Boteler, D. H. and Pirjola, R. J.: 1998, *Geophys. J. Int.* 132, 31.
- Gopalswamy, N.: 2004, in: Poletto, G., Suess, S.T. (Eds.), *The Sun and the Heliosphere as an Integrated System*. Kluwer, Dordrecht, 201.
- Gosling, J.T., Hansen, R.T. and Bame, S.J.: 1971, *J. Geophys. Res.* 76, 1811.
- Hildner, E., Gosling, J.T., MacQueen, R.M., Munro, R.H., Poland, A.I. and Ross, C.L.: 1976, *Sol. Phys.* 48, 127.
- Hodgson, R.: 1859, *Monthly Notices of the Royal Astronomical Society* 20, 15.
- Liu, C., Li, Y. and Pirjola, R.: 2014, *J. Space Weather Space Clim.* 4, A03, doi:10.1051/swsc/2013057
- Matandirotya, E., Cilliers, P. J. and Van Zyl, R.R.: 2015, *Space Weather* 13, 185, doi: 10.1002/2014SW001135.
- Pirjola, R. and Viljanen, A.: 1998, *Ann. Geophysicae* 16, 1434.
- Torta, J.M., Marsal, S. and Quintana, M.: 2014, *Earth, Planets and Space* 66:87.
- Viljanen, A. and Pirjola, R.: 1989, *J. Geomag. Geoelectr.* 41, 411.
- Viljanen, A.: 1997, *Geophys. Res. Lett.* 24, 631.
- Viljanen, A., Pirjola, R., Wik, M., Adam, A., Pracser, E., Sakharov, Y. and Katkalov, J.: 2012, *J. Space Weather Space Clim.* 2, A17, doi: 10.1051/swsc/2012017.
- Viljanen, A., Pirjola, R., Pracser, E., Katkalov, J. and Wik, M.: 2014, *J. Space Weather Space Clim.* 4, A09, doi: 10.1051/swsc/2014006.
- Watari, S.: 2015, *Earth, Planets and Space* 67:77, doi:10.1186/s40623-015-0253-8.
- Wei, L.H., Homeier, N. and Gannon, J.L.: 2013, *SpaceWeather* 11, 451, doi:10.1002/swe.20073.